

# Modeling Human Visual Search: A Combined Bayesian Searcher and Saliency Map Approach for Eye Movement Guidance in Natural Scenes

Melanie Sclar<sup>1\*</sup>, Gastón Bujia<sup>1,2\*</sup>, Sebastián Vita<sup>1</sup>, Guillermo Solovey<sup>2</sup>,  
Juan Esteban Kamienkowski<sup>1,3</sup>

<sup>1</sup> Laboratorio de Inteligencia Artificial Aplicada, Instituto de Ciencias de la Computación, Universidad de Buenos Aires – CONICET, Argentina

<sup>2</sup> Instituto del Cálculo, Universidad de Buenos Aires – CONICET, Argentina

<sup>3</sup> Departamento de Física, FCEyN, Universidad de Buenos Aires, Argentina

## Abstract

Finding objects is essential for almost any daily-life visual task. Saliency models have been useful to predict fixation locations in natural images, but are static, i.e., they provide no information about the time-sequence of fixations. Nowadays, one of the biggest challenges in the field is to go beyond saliency maps to predict a sequence of fixations related to a visual task, such as searching for a given target. Bayesian observer models have been proposed for this task, as they represent visual search as an active sampling process. Nevertheless, they were mostly evaluated on artificial images, and how they adapt to natural images remains largely unexplored.

Here, we propose a unified Bayesian model for visual search guided by saliency maps as prior information. We validated our model with a visual search experiment in natural scenes recording eye movements. We show that, although state-of-the-art saliency models perform well in predicting the first two fixations in a visual search task, their performance degrades to chance afterward. This suggests that saliency maps alone are good to model bottom-up first impressions, but are not enough to explain the scanpaths when top-down task information is critical. Thus, we propose to use them as priors of Bayesian searchers. This approach leads to a behavior very similar to humans for the whole scanpath, both in the percentage of target found as a function of the fixation rank and the scanpath similarity, reproducing the entire sequence of eye movements.

## Introduction

Visual search is a natural task that humans perform in everyday life, from looking for someone in a photograph to searching where you left your favorite mug in the kitchen. Finding our goal relies on our ability to gather visual information through a sequence of eye movements, performing a discrete sampling of the scene. This sampling of information is not carried out on random points. The fixations of the gaze follow different strategies, trying to minimize the number of steps needed to find the target (Borji and Itti 2014; Rolfs 2015; Tatler et al. 2010; Yarbus 1967). This process is a classical example of the active sensing or

sampling paradigm, where humans perform decisions about the different ways of sampling information making inferences with the gathered information so far, in order to fulfill a necessity (Yang, Wolpert, and Lengyel 2016; Gottlieb and Oudeyer 2018). This way, each decision is expected to reduce uncertainty about the environment (Gottlieb and Oudeyer 2018; Najemnik and Geisler 2005). Moreover, this decision-making behavior depends on the purpose; for instance, whether it is task-driven or simple curiosity. Predicting the eye movements necessary to meet a goal is a computationally-complex task since it must combine the bottom-up information capturing processes and the top-down integration of information and updating of expectations in each fixation.

A related task is the prediction of the most likely fixation positions in the scene, whose purpose is to build a *saliency map*, identifying regions that draw our attention within an image. The first saliency models were built based on computer vision strategies, combining different filters over the image (Itti and Koch 2001). Some of these filters could be very general, such as a low-pass filter that gives the idea of the horizon (Itti, Koch, and Niebur 1998; Torralba and Sinha 2001), or more specific, such as detecting high-level features like faces (Cerf et al. 2008). In recent years, deep neural networks (DNNs) have advanced the development of saliency maps. Many saliency models have successfully incorporated pre-trained convolutional DNNs in order to extract low and high-level features of the images (Kummerer et al. 2017; Cornia et al. 2016, 2018). These novel approaches were summarized in MIT/Tuebingen’s collaboration website (Kummerer, Wallis, and Bethge 2018). Nevertheless, they produce accurate results only in the first few fixations of free exploration tasks (Torralba et al. 2006) as they cannot make use of the sequential nature of the task nor combine information through the sequence of fixations. Thus, they may not be able to replicate their good results when performing a complex task, such as a visual search.

Recently, Zhang et al. (2018) proposed an extension of those models to predict the sequence of fixations in a visual search in natural images. They use a greedy algorithm based on DNNs, mimicking the behavior of the visual system by elaborating an attention map related to the search goal. Using a greedy algorithm implied forcing some known behav-

\*Indicates equal contribution. Correspondence should be addressed to M.S. (melaniesclar@gmail.com) or G.B. (gastonbujia@gmail.com).

iors of human visual search –like inhibition of return– that arise naturally with longer-sighted objective functions.

Nowadays, there is a growing interest in Bayesian models given their good results at modeling human behavior and also for having straightforward interpretations related to human information processing (Ullman 2019). For instance, different Bayesian Models were applied to decision making or perceptual tasks (O’Reilly, Jbabdi, and Behrens 2012; Rohe and Noppeney 2015; Samad, Chung, and Shams 2015; Wiecki, Poland, and Frank 2015; Turgeon, Lustig, and Meck 2016; Knill and Pouget 2004; Tenenbaum, Griffiths, and Kemp 2006; Meyniel, Sigman, and Mainen 2015). In the case of visual search, Najemnik and Geisler (2005) have proposed a model that decides the next eye movement based on its prior knowledge, a visibility map, and the current state of a posterior probability that is updated after every fixation. In this model, inhibition of return, moderate saccade length, among other human characteristics of visual search arise naturally (Najemnik and Geisler 2005). The results of this Ideal Bayesian searcher (IBS) have had a wide impact, but the images they used in their experiments were all artificial. Recently, Hoppe and Rothkopf (2019) proposed a visual search model that incorporates planning. It uses the uncertainty of the current observation to select the upcoming gaze locations in order to maximize the probability of detecting the location of the target after the sequence of two saccades. As Najemnik and Geisler (2005), their task is specifically designed for maximizing the difference between models, i.e. finding the target in very few fixations on artificial stimuli. In order to extend these results to natural images, it is necessary to incorporate the information available in the scene.

Here, we show that an IBS model combined with state-of-the-art saliency maps as priors performs similarly to humans in a visual search task on natural scenes. Moreover, we incorporate a different update rule to the IBS model, based on a correlation for the template response. This modification could incorporate the effect of distractors, even though we did not specifically test this hypothesis in our experiments. We also simplify assumptions from prior work by avoiding to measure each subjects’ visibility map beforehand, and having an *a priori* approximation instead. Previous work compares the general performance between humans and the model (targets found and total number of fixations). Moving one step further, we quantitatively compare the scanpaths (ordered sequence of fixations) produced by the model with the ones recorded by human observers.

## Visual search in natural indoor images:

### Human data

#### Paradigm and human data acquisition and preprocessing

We set up a visual search experiment in which participants have to search for an object in a crowded indoor scene. First, the target was presented in the center of the screen, subtending  $144 \times 144$  pixels of visual angle (Fig. S1). After 3 seconds, the target was replaced by a fixation dot at a pseudo-random position at least 300 pixels away from the actual tar-

get position in the image (Fig. S1). This was done to avoid starting the search too close to the target. The initial position was the same for a given image and all participants. The search image appears after the participant fixates the dot. Thus, all observers initiate the search in the same place for each image. (Fig. S1).

Saccades and fixations were parsed online. The search period finishes when the participant fixates the target or after  $N$  saccades, allowing an extra 200ms, in order to allow observers to process information of this last fixation (Kotowicz, Rutishauser, and Koch 2010). The maximum number saccades allowed ( $N$ ) varied between 2, 4, 8, 12. These values were randomized for each participant, independently of the image. The experiment was programmed using PsychToolbox and EyeLink libraries in MATLAB (Brainard 1997; Kleiner, Brainard, and Pelli 2007).

The images correspond to 134 indoor pictures from Wikimedia commons, indoor design blogs, and LabelMe database (Russell et al. 2008), which have several objects and no human figures or text. The image was presented at a  $1024 \times 768$  resolution (subtending  $28.3 \times 28.8$  degrees of visual angle). For each image, a single target was selected among objects of size equal or less than  $72 \times 72$  pixels. Also, we excluded targets with almost exact copies within the image (i.e. a cup within a set of cups) to prevent high working memory requirements from humans. For all of them we considered a surrounding region of  $72 \times 72$  pixels. Finally, we checked that there were no consistent spatial biases across the images.

Fifty-seven subjects (34 male; age  $25.1 \pm 5.9$  years old) participated in the Visual Search task. All were students or teachers from the Facultad de Ciencias Exactas y Naturales de la Universidad de Buenos Aires. All subjects were naive to the objectives of the experiment, had normal or corrected-to-normal vision, and provided written informed consent according to the recommendations of the declaration of Helsinki to participate in the study.

See more details on the paradigm and data acquisition and preprocessing in Supplemental Information.

### Human behavior results

During the experiment, observers have to search for a given target object within natural indoor scenes. The trial stops when the observers find the target or after  $N$  saccades ( $N = 2, 4, 8, 12$ ). As expected, the proportion of targets found increases as a function of the saccades allowed (Fig. 1A), reaching a plateau from 8 to 12 saccades allowed and on (Fig. 1A and data from a preliminary experiment with up to 64 saccades not shown).

Overall, eye movements recorded behave as expected. First, the amplitude decreases with the fixation rank, presenting the so-called coarse-to-fine effect (Fig. 1B), and the saccades tended to be horizontal more than vertical (Fig. 1C). Finally, the initial spatial distribution of fixations had a central bias, and then extended first over the horizon until it covered the whole image, as the targets are uniformly distributed along the scene (Fig. 1D). This effect could be partially due to the organization of the task (the central drift correction and presentation of the target), the setup (the central

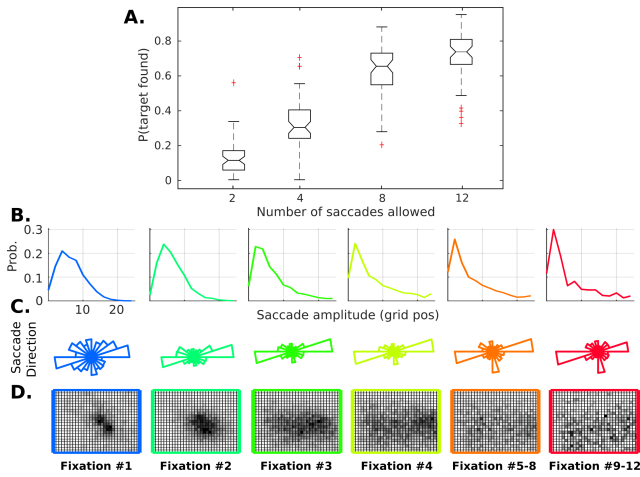


Figure 1: General behavior. (A) Proportion of targets found as a function of the number of saccades allowed. Distributions of (B) saccade length, (C) saccade direction (measured in degrees from the positive horizontal axis), and (D) fixations’ position for different fixation ranks (1,2,3,4,5-8,9-12).

position of the monitor with respect of the eyes/head), and the images (the photographer typically centers the image); it also could be due to processing benefits, as it is the optimal position to acquire low-level information of the whole scene or to start the exploration.

## Searcher Modeling Approach

The proposed model involves two main aspects of the visual search implementation: a saliency map estimation step as a first, glimpse-like, information extraction, and successive search steps in order to build the full scanpath.

### Exploring saliency maps

The saliency maps were usually estimated in a scene-viewing task, where observers freely moved their eyes, exploring whatever captured their interests. The motivation of using the full saliency as prior in a visual search task lies in the results of the flash-preview moving-window paradigm that shows that even less than a few hundreds of milliseconds’ glimpse of a scene can guide search as long as sufficient time is subsequently available to combine prior knowledge with the current visual input (Oliva and Torralba 2006; Torralba et al. 2006; Castelano and Henderson 2007). Importantly, it was also shown that this is more relevant in the first saccades of a full scene search, and its predictive power decays with the fixation rank (Torralba et al. 2006).

**Saliency Maps** In the last few years several saliency models appeared in the literature and made their code available. Many of those were nicely summarized and compared in the <https://saliency.tuebingen.ai/> repository (Judd, Durand, and Torralba 2012; Kummerer, Wallis, and Bethge 2018; Bylinskii et al. 2018). With the purpose of understanding which features guide the search in this section, we choose and compare five different state-of-the-art

saliency maps for our task: DeepGaze 2 (Kummerer et al. 2017), MLNet (Cornia et al. 2016), SAM-VGG and SAM-ResNet (Cornia et al. 2018), and ICF (Intensity Contrast Feature) (Kummerer et al. 2017).

All the saliency models considered (except for ICF) are based on neural network architectures, using different convolutional networks (CNN) pretrained on object recognition tasks. These CNNs played the role of calculating a fixed feature space representation (feature extractor) for the image which then will be fed to a predictor function (in the models we consider, also a neural network). DeepGaze uses a VGG-19 (Simonyan and Zisserman 2014) as feature extractor, and the predictor is a simpler four-layer CNN (Kummerer et al. 2017). The MLNet model uses a modified VGG-16 (Simonyan and Zisserman 2014) that returns several feature maps, and a simpler CNN is used as a predictor that incorporates a learnable center prior (Cornia et al. 2016). Finally, SAM could use both VGG-16 and ResNet50 (He et al. 2016) as two different feature extractors, and the predictor is a neural network with attentive and convolutional mechanisms (Cornia et al. 2018). ICF has a similar architecture to DeepGaze, but it uses Gaussian filters instead of a neural network. This way, ICF extracts purely low-level image information (intensity and intensity contrast). We also include a saliency model with just the center bias, modelled by a 2D Gaussian distribution.

As the control model, we built a human-based saliency map using the accumulated fixation position of all observers for a given image, smoothed with a Gaussian kernel (st. dev. = 25 ppx). Given that observers were forced to begin each trial in the same position, we did not use the first fixations but the third. This way we capture the regions that attract human attention.

**Prediction of observers’ fixation positions** We evaluated how just the saliency models perform in predicting fixations along the search by themselves. Thus, we considered each saliency map  $S$  as a binary classifier on every pixel and used Receiver Operator Curves (ROC) and Area Under the Curve (AUC) to measure their performance. This comes with the difficulty that there is not a unique way of defining the false positive rate (**fpr**). In dealing with this problem, previous work on this task has used many different definitions of (ROC and its corresponding) AUC (Borji et al. 2013; Riche et al. 2013; Bylinskii et al. 2018; Kummerer, Wallis, and Bethge 2018). Briefly, to build our ROC we considered the true positive rate (**tpr**) as the proportion of saliency map values above each threshold at fixation locations and the **fpr** as the proportion of saliency map values above threshold at non-fixated pixels (Fig. 2A).

As expected, the saliency map built from the distribution of third fixations performed by humans (human-based saliency map) is superior to all other saliency maps, and the center bias map was clearly worse than the rest of them (Fig. 2B). This is consistent with the idea that the first steps in visual search are mostly guided by image saliency. The rest of the models have similar performance on AUC, with DeepGaze2 performing slightly better than the others (Fig. 2B). Using different definitions of AUC (Borji et al. 2013;

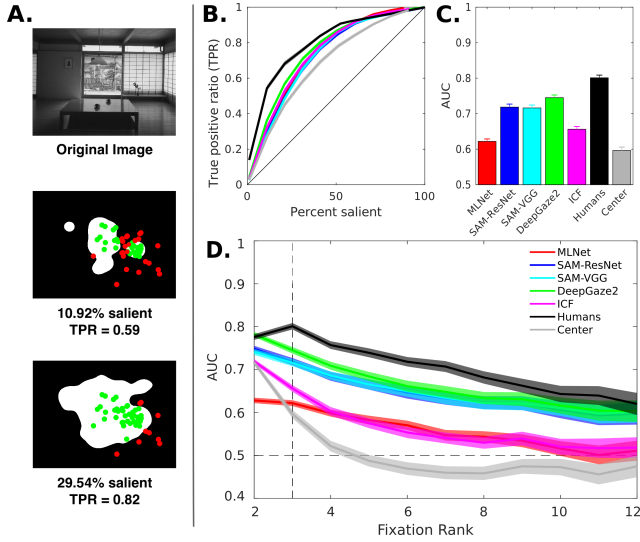


Figure 2: Saliency maps. **A)** Example on how to estimate the TPR for the ROC curve, **B)** ROC curves and **C)** AUC values for the third fixation and **D)** AUC for each Model as a function of the current Fixation Rank. Color mapping for models is consistent over B, C, and D.

Riche et al. 2013; Bylinskii et al. 2018; Kummerer, Wallis, and Bethge 2018) showed the same trend (Table S1). If we consider all fixations the AUC is reduced for all models, including the human-based saliency map built on the third fixations (Fig. S2).

All models reached a maximum in AUC values at the second fixation except the human-based model that peaked at the third fixation as expected (Fig. 2C). Interestingly, the center bias begins at a similar level as the other saliency maps but decays more rapidly, reaching 0.5 in the fourth fixation. Thus, other saliency maps must capture some other relevant visual information. Nevertheless, the AUC values from all saliency maps decay smoothly (Fig. 2C). This suggests that the gist the observers are able to collect in the first fixations is largely modified by the search. Top-down mechanisms must take control and play major roles in eye movement guidance as the number of fixations increase (Itti and Koch 2000). The DeepGaze 2 model performed better over all fixation ranks, becoming indistinguishable from human performance in the second fixation (Fig. 2C).

### Bayesian Searcher models

In the previous section, we showed that saliency models alone are not able to predict the fixation positions in a visual scene when a task, even a simple task like visual search, is performed. Moreover, these models are not developed to predict the order of those fixations. In the next section, we develop models that integrate the saliency maps as priors but have rules implemented to update those probabilities as the search progresses.

**Description of the Ideal Bayesian searcher (IBS)** Najmnik and Geisler (2005)’s IBS computes the optimal next

fixation location in each step. It considers each possible next fixation and picks the one that will maximize the probability of correctly identifying the location of the target after the fixation. The decision of the optimal fixation location at step  $T + 1$ ,  $k_{opt}(T + 1)$ , is computed as (eq. 1):

$$k_{opt}(T + 1) = \underset{k(T+1)}{\operatorname{argmax}} \sum_{i=1}^n p_i(T) p(C|i, k(T + 1)) \quad (1)$$

where  $p_i(T)$  is the posterior probability that the target is at the  $i$ -th location within the grid after  $T$  fixations and  $p(C|i, k(T + 1))$  is the probability of being correct given that the true target location is  $i$ , and the location of the next fixation is  $k(T + 1)$ .  $p_i(T)$  involves the prior, the visibility map ( $d'_{ik(T)}$ ) and a notion of the target location ( $W_{ik(t)}$ ):

$$p_i(T) = \frac{\operatorname{prior}(i) \cdot \prod_{t=1}^T \exp(d'^2_{ik(t)} W_{ik(t)})}{\sum_{j=1}^n \operatorname{prior}(j) \cdot \prod_{t=1}^T \exp(d'^2_{jk(t)} W_{jk(t)})} \quad (2)$$

The template response,  $W_{ik(t)}$ , quantifies the similarity between a given position  $i$  and the target image from the fixated position  $k(t)$  ( $t$  is any previous fixation). It is defined as  $W_{ik(t)} \sim \mathcal{N}(\mu_{ik(t)}, \sigma_{ik(t)}^2)$  where:

$$\mu_{ik(t)} = \mathbb{1}_{(i = \text{target location})} - 0.5, \quad \sigma_{ik(t)} = \frac{1}{d'_{ik(t)}} \quad (3)$$

Abusing notation, in eq. 2  $W_{ik(t)}$  refers to a value drawn from this distribution.

IBS has only been tested in artificial images, where subjects need to find a gabor patch among  $1/f$  noise in one out of 25 possible locations. This work is, to our knowledge, the first one to test this approach in natural scenes. Below, we discuss the modifications needed to apply IBS to eye movements in natural images.

**Modifications to the IBS to handle natural scenes (correlation-based IBS (cIBS)).** Since it would be both computationally intractable to compute the probability of fixating in every pixel of a  $1024 \times 768$  image, and ineffective to do so –as useful information span over regions larger than a pixel–, we restrict the possible fixation locations to be analyzed to the center points of a grid of  $\delta \times \delta$  pixels each. We collapse the eye movements to these points accordingly: consecutive fixations within a cell were merged into one fixation to be fair with the model behavior.

The original IBS model had a uniform prior distribution. Since we are trying to model fixation locations in a natural scene, we introduced a saliency model as the prior. The  $\operatorname{prior}(i)$  will be the average of the saliency in the  $i$ -th grid cell.

Importantly, the presence of the target in a certain position in natural images is not as straightforward as in artificial stimuli, where all the incorrect locations were equally dissimilar. In natural images there are often distractors, i.e. positions in the image that are visually similar to the target, especially if seen with low visibility. Therefore, we propose

a redefined template response  $\tilde{W}_{ik(t)} \sim \mathcal{N}(\tilde{\mu}_{ik(t)}, \tilde{\sigma}_{ik(t)}^2)$ , where  $\tilde{\mu}_{ik(t)} \in [-1, 1]$  is defined as (eq. 4):

$$\tilde{\mu}_{ik(t)} = \mu_{ik(t)} \cdot \left( d'_{ik(t)} + \frac{1}{2} \right) + \text{corr}_i \cdot \left( \frac{3}{2} - d'_{ik(t)} \right) \quad (4)$$

$\text{corr}_i \in [-0.5, 0.5]$  is the cross-correlation of location  $i$  and the target image, used as a measure of image similarity.

Moreover, we modified  $\sigma_{ik(t)}$  to keep the variance depending on the visibility, but we incorporate two parameters (eq. 5):

$$\tilde{\sigma}_{ik(t)} = \frac{1}{a \cdot d'_{ik(t)} + b} \quad (5)$$

The parameters  $a$  and  $b$  jointly modulate the inverse of the visibility and prevent  $1/d'$  from diverging. These parameters were not included in the original model probably because  $d'$  was estimated empirically (from thousands of trials and independently for each subject) and the  $d'$  was never exactly equal to zero. Recently, Bradley, Abrams, and Geisler (2014) simplified the task by fitting a visibility map built from a first-principle model which proposed an analytic function with several parameters, that should still be fitted for each participant. Here, we further simplified it by using a two-dimensional Gaussian with the same parameters for every participant, avoiding a potential leak of information about the viewing patterns to the model. The parameters were taken *a priori* (estimated from parameters in Najemnik and Geisler (2005); Bradley, Abrams, and Geisler (2014)). We chose the parameters of the model using a classical grid search procedure in a previous experiment with a smaller dataset and the same best parameters ( $\delta = 32$ ,  $a = 3$  and  $b = 4$ ) are used for all the models.

Finally, since we are trying to model fixation locations in a natural scene, we introduced a saliency model as the initial prior instead of an uniform distribution used by the original model. The *prior*( $i$ ) will be the average of the saliency in the  $i$ -th grid cell.

We call this variation of the model *correlation-based IBS* (cIBS). The data, models and code will be publicly available upon publication. It is worth mentioning that, to our knowledge, not only an implementation of the Najemnik and Geisler (2005) model is publicly available for the first time here, but also it is largely optimized. More details in Supplemental Information.

**Evaluating searcher models on human data** We first evaluate the updating of probabilities and the decision rule of the next fixation position of the proposed *cIBS* model. For comparison, we used the previous *IBS* model, in which the *template response* accounts only for the presence or not of the target, and not for the similarity of the given region with the target. Also, we implemented two other basic models: a *Greedy searcher* and a *Saliency-based searcher*. The *Greedy searcher* bases its decision on maximizing the probability of finding the target in the next fixation. It only considers the present posterior probabilities and the visibility map, and does not take into account how the probability map is going to be updated after that. The *Saliency-based searcher* simply goes through the most salient regions of the image, adding an inhibition-of-return effect to each visited region.

In these models, we used the DeepGaze2 as a prior, because it is the best performing saliency map of the previous section. We also evaluate the usage of different priors with the cIBS model, comparing with the center bias alone, which is a centered two-dimensional Gaussian distribution, a uniform (flat) distribution, and a white noise distribution.

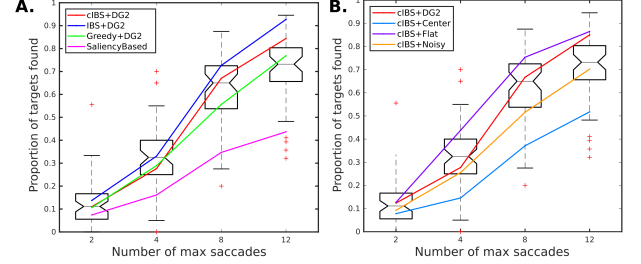


Figure 3: Model performance comparison. Proportion of target found for each threshold considered. The boxes represent the human behaviour distribution. The curves are the performance achieved by the models considered using different search strategies (A) with DeepGaze2 (DG2) as prior and different priors (B) using cIBS strategy.

The proportion of targets found for any of the possible saccades allowed was used as a measure of the overall performance (Fig. 3). In Table 1 we summarize the metrics comparing humans and models. The Weighted Distance measures the mean difference between curves (Fig. 3). The Jaccard index represents the proportion of targets found by the model to the total targets found by the subjects, and the Mean Agreement metric measures the proportion of trials where subject and model had the same performance: both, subject and model, found (or not) the target (See Supplemental Information). When comparing different searchers with the same prior, cIBS has the best agreement with the humans’ performance as a compromise of different metrics (Table 1). In particular, the performance of cIBS+DeepGaze2 is the closest to the human mean agreement ( $0.65 \pm 0.086$ ). Nevertheless, the curves of the IBS and Greedy models were also very close to humans (Fig 3A) and each of them performed better in one metric (Table 1). It is important to note that Weighted Distance significantly improves when adding the distractor component (cIBS vs IBS).

Only the basic Saliency-based model had poorer agreement with the human performance, showing that template matching weighted by visibility is a plausible mechanism for searching potential targets in the scene.

Then, we explored the importance of the prior, comparing the best searcher model with the chosen prior against the different basic priors. Again, the cIBS+DeepGaze2 had better overall agreement with humans’ behavior (Fig. 3B and Table 1) and, interestingly, is the only model that presented a step-like function characteristic from humans (Fig. 3B).

Going one step further, we compare the scanpaths using the *scanpath dissimilarity* pairwise metric proposed by Jarodzka, Holmqvist, and Nyström (2010). Briefly, the scanpath metric represent them as time-aligned vectors, each scanpath



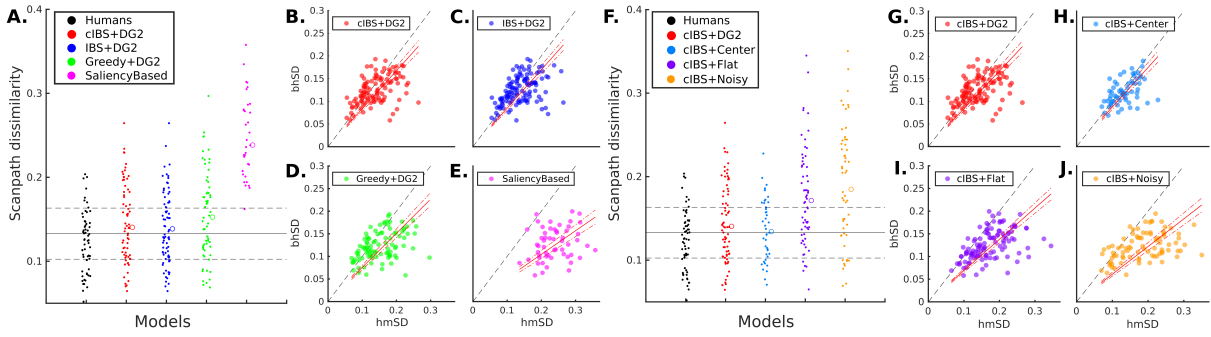


Figure 4: Human-model scanpath dissimilarity comparison. All metrics are computed first between each pair of participants/model and then averaged. A) Distribution of scanpath dissimilarity between humans and different search strategies using DeepGaze2 as prior. Each dot represents a trial image. B-E) Distribution of scanpath dissimilarity between humans ( $bhSD$ ) and humans-model ( $hmSD$ ) for each trial image. F) Distribution of scanpath dissimilarity between different priors using cIBS as search strategy. G-J) Same plot as (B-E) for each different prior considered. Only correct trials were considered in (B-E, G-J).

is defined as a sequence of fixations  $u_i$  ( $(x,y)$ -coordinates) where the  $i$ -th saccade is the shortest path (vector) going from  $u_i$  to  $u_{i+1}$ . Each  $u_i$  may not be exactly a fixation, but the center of a cluster of several fixations, making this measure more robust. Depending on the objective of the comparison, it could be used with different summary measures based on those characteristics. As we aim to compare the sequence of explored locations between humans and our model, we use shape dissimilarity. It is calculated as the normalized difference between the saccade vectors, where a scanpath dissimilarity of 0 indicates that the scanpaths are highly similar, and 1 indicates that there is no correspondence between them.

We started comparing between searcher models, both cIBS and IBS were almost indistinguishable from humans, the Greedy model was still very close, and only the Saliency-based model resulted in a significantly different behavior (Fig. 4A-E). We quantified this relation by measuring the correlation and the slope of a linear regression (with null intercept) of the dissimilarity between humans ( $bhSD$ ) and between humans and the model ( $hmSD$ ) (Table 1). The rationale of these measures is that the ground truth of each image (the human scanpath) has different variability across images, and we cannot expect that in the case of very diverse scanpaths (higher dissimilarity) among humans, the model was close to all of them. A close look at the correlation between the dissimilarity measure in humans and models evidenced that there were only a small fraction of images that departed from the human’s scanpaths (Fig. 4B-E). These images (1% using  $\mu + 3\sigma$  for cIBS+DG2) correspond to cases where few people found the target or, interestingly, where there are different possible scanpath behaviors (i.e. some people start looking for a cup on the cupboard and others on the table) (Supplemental Figure S3). Further studies should be performed to explore individual differences between observers.

When comparing between priors, we observed that both the models with DeepGaze2 and Center priors were closer to humans’ values, and the flat and noisy priors had larger scanpath dissimilarities (Fig 4F). The model with a flat

prior had a slightly better correlation, but both the models with DeepGaze2 and Center priors had good correlation and slopes closer to 1 (Table 1). This suggests that the initial center bias is a fair approximation of the human priors. Nonetheless, although both scanpaths were almost indistinguishable from humans, saliency adds some information that makes the model with DeepGaze2 quite better in finding the target.

## Conclusions

We introduced the cIBS model, an expansion of the IBS model to face natural scenes. In summary, we used saliency maps as priors to model the information collected in the first glimpse that guides the first saccades, and we modified the computation of the *template response* to be able to, first, use a simpler model of visibility and, second, give graded responses to regions similar to the target, incorporating the notion of distractors. To evaluate the model, we created a dataset of 57 subjects searching on 134 images, where we compared cIBS to IBS and other strong baselines. We observed that saliency models performed well in predicting initial fixations, in particular the third fixation. Humans seemed to start from the initial forced fixation position, move to the center, and then to the most (bottom-up) salient location. After that, the performance of all the saliency models decay to almost chance, as is expected from their conception. They mainly encode bottom-up information of the image (Itti and Koch 2000) and not the aim of the task, and they are not able to change and update as it progresses. This is also consistent with previous results from Torralba et al. (2006) who implement a saliency model for a visual search task.

As saliency models are good in predicting first bottom-up impressions, they are ideal candidates to be included as priors in the proposed Bayesian framework. The central bias performed well in the first two fixations, and is included in all the saliency models (Cornia et al. 2016, 2018; Kummerer et al. 2017). The central bias by itself resulted in a good prior in terms of scanpath similarity but not in the performance of finding the target. However, the DeepGaze2 had the better compromise of both measures. This suggests that bottom-

Searcher:	IBS	Greedy	Saliency	cIBS	cIBS	cIBS	cIBS
Prior:	DG2	DG2	DG2	DG2	Center	Flat	Noisy
Weighted Distance	0.78	0.13	2.14	0.31	1.38	0.72	0.15
Mean Agreement	0.64 (0.096)	0.63 (0.082)	0.55 (0.092)	0.64 (0.084)	0.60 (0.086)	0.60 (0.109)	0.61 (0.082)
Jaccard Index	0.54 (0.105)	0.47 (0.091)	0.32 (0.073)	0.51 (0.098)	0.38 (0.086)	0.51 (0.109)	0.46 (0.089)
Linear Regression	0.85	0.76	0.52	0.84	0.88	0.69	0.61
$\rho$	0.48	0.44	0.22	0.50	0.50	0.54	0.43

Table 1: Different measures on performance and scanpath dissimilarity between humans and models. *Weighted Distance* is the distance between humans and model performance weighted by humans dispersion. *Mean Agreement* and *Jaccard Index* measure coincidence of humans and model’s correct target detections (See Supplemental Information). *Linear Regression* corresponds to the slope of a simple  $y \sim x$  model between humans scanpaths dissimilarity (bhSD in Fig 4 B-E and G-J) and models scanpaths dissimilarity (hmSD in Fig 4 B-E and G-J).  $\rho$  is the Spearman’s correlation coefficient between scanpath dissimilarities bhSD and hmSD. Only correct trials were considered and averaged for each image ( $N = 134$ ).

up cues provided by the saliency maps are relevant to the search.

Regarding the update and decision mechanism, it is clear that the simple saliency-based searcher, i.e. wandering around the most salient regions until bumping into the target, is not a good model of visual search. Humans use not only information of the scene but also information about the target and previous fixations. Then, a rule of comparing peripheral information of the scene and the target should be implemented, along with a mechanism for combining that information. Those mechanisms are implemented in the Greedy, IBS, and cIBS models, with the difference that the Greedy model maximizes the probability of finding the target in the next fixation, and the IBS and cIBS maximize the probability of finding the target after the next fixation. Overall, the Greedy model had worse performance than both IBS and cIBS models, suggesting that humans actually implement longer plans when searching in a visual scene. When comparing Bayesian models, we showed that when searching in a cluttered image it’s important to account for the distractors present in the scene, extending the previous proposal from Najemnik and Geisler (2005).

Previous efforts on including contextual information aimed mainly to predict image regions likely to be fixated. For instance, they combined statically a spatial filter-based saliency map with previous knowledge of target object positions on the scene (Torralla et al. 2006). Some other works aimed to predict the sequence of fixations, but efforts on non-Bayesian modeling mainly used greedy algorithms (Rasouli and Tsotsos 2014; Zhang et al. 2018). Here, we compared an example of greedy algorithm with others with a more long-sighted objective function, which has the additional benefit of having some known behaviors of human visual search arise naturally. For example, Zhang et al. (2018) forced inhibition of return, while our model has it implicitly incorporated. Crucially, Bayesian frameworks are highly interpretable and connect our work to other efforts in modeling top-down influences in perception and decision-making.

It’s also important to note that, although the Najemnik and Geisler (2005) model was a very insightful and influential proposal, to our knowledge, our work is the first one that uses a Bayesian framework to predict eye movements

during visual search in natural images. It is a leap in terms of applications since prior work on Bayesian models was done in very constrained artificial environments (looking for a tiny Gabor patch embedded in background  $1/f$  noise) (Najemnik and Geisler 2005). Moreover, we addressed possible modifications when considering the complexities of natural images. Specifically, the addition of a saliency map as prior, the modification of the template response’s mean, and shift in visibility. We also simplified assumptions from Najemnik and Geisler (2005) by not having to measure each person’s visibility map beforehand. We use the same visibility map across subjects, which also avoids a potential leak of information about the viewing patterns to the model. Finally, we also share an optimized code for the models which would be useful for others to replicate both Najemnik and Geisler (2005) and our results.

Our model aligns with the work of many researchers that propose probabilistic solutions to model human behavior from first principles. For instance, Bruce and Tsotsos (2006, 2009) proposed a saliency model based on information maximization principle, which demonstrates great efficacy in predicting fixation patterns across both pictures and movies. Also, Ma et al. (2011) implement a near-optimal visual search model for a fixed-gaze search task (i.e. exploring the allocation of covert attention), extending previous models to deal with the reliability of visual information across items and displays, and proposing an implementation of how information should be combined across objects and spatial location, through marginalization. Interestingly, in both attempts to explain overt and covert allocation of attention they proposed an implementation through physiologically plausible neural networks.

More generally, the present work expands the general growing notion of the brain as an organ capable of generalizing and performing inferences in noisy and cluttered scenarios through Bayesian inference, building complete and abstract models of its environment. Nowadays, those models cover a broad spectrum of perceptual and cognitive functions, such as decision making and confidence, learning, multisensorial perception, and others (Knill and Pouget 2004; Tenenbaum, Griffiths, and Kemp 2006; Meyniel, Sigman, and Mainen 2015).

## Code / Data availability

Code, data, and chosen parameters will be made publicly available upon publication for full reproduction of our results. Data will include the image dataset with targets, as well as fixation data for all of the subjects.

## Author contributions

M.S. prepared the indoor images/targets dataset and coded the first implementation of the presented models, including numerical optimizations and speed-ups. M.S., G.S. and J.K. designed the task, collected the human data and defined the model idea. G.B. and S.V. pruned the model's code, extended it and explored their parameters. M.S., G.B., S.V. and J.K. performed the analysis. The manuscript was written by G.B., M.S. and J.K.

## Acknowledgments

We thank P Lagomarsino and J Laurino for their collaboration with the data acquisition, C Diuk (Facebook), A Salles (OpenZeppelin) and Matias J Ison (Univ. of Nottingham, UK) for their feedback and insight on the work, and K Ball (UT Austin) for English editing of this article. The authors were supported by the National Science and Technology Research Council (CONICET) and the University of Buenos Aires (UBA). The research was supported by the ARL (W911NF-19-2-0240), UBA (20020170200259BA), and the National Agency of Promotion of Science and Technology (PICT 2016-1256).

## References

- Borji, A.; and Itti, L. 2014. Defending Yarbus: Eye movements reveal observers' task. *Journal of vision* 14(3): 29–29.
- Borji, A.; Tavakoli, H. R.; Sihite, D. N.; and Itti, L. 2013. Analysis of scores, datasets, and models in visual saliency prediction. In *Proceedings of the IEEE international conference on computer vision*, 921–928.
- Bradley, C.; Abrams, J.; and Geisler, W. 2014. Retina-v1 model of detectability across the visual field. *Journal of vision* 14(12): 22–22.
- Brainard, D. H. 1997. The Psychophysics Toolbox. *Spatial Vision* 10: 433–436.
- Bruce, N.; and Tsotsos, J. 2006. Saliency based on information maximization. In *Advances in neural information processing systems*, 155–162.
- Bruce, N. D.; and Tsotsos, J. K. 2009. Saliency, attention, and visual search: An information theoretic approach. *Journal of vision* 9(3): 5–5.
- Bylinskii, Z.; Judd, T.; Oliva, A.; Torralba, A.; and Durand, F. 2018. What do different evaluation metrics tell us about saliency models? *IEEE transactions on pattern analysis and machine intelligence* 41(3): 740–757.
- Castelhano, M. S.; and Henderson, J. M. 2007. Initial scene representations facilitate eye movement guidance in visual search. *Journal of Experimental Psychology: Human Perception and Performance* 33(4): 753.
- Cerf, M.; Harel, J.; Einhäuser, W.; and Koch, C. 2008. Predicting human gaze using low-level saliency combined with face detection. In *Advances in neural information processing systems*, 241–248.
- Cornia, M.; Baraldi, L.; Serra, G.; and Cucchiara, R. 2016. A deep multi-level network for saliency prediction. In *2016 23rd International Conference on Pattern Recognition (ICPR)*, 3488–3493. IEEE.
- Cornia, M.; Baraldi, L.; Serra, G.; and Cucchiara, R. 2018. Predicting human eye fixations via an lstm-based saliency attentive model. *IEEE Transactions on Image Processing* 27(10): 5142–5154.
- Gottlieb, J.; and Oudeyer, P.-Y. 2018. Towards a neuroscience of active sampling and curiosity. *Nature Reviews Neuroscience* 19(12): 758–770.
- He, K.; Zhang, X.; Ren, S.; and Sun, J. 2016. Deep residual learning for image recognition. In *Proceedings of the IEEE conference on computer vision and pattern recognition*, 770–778.
- Hoppe, D.; and Rothkopf, C. A. 2019. Multi-step planning of eye movements in visual search. *Scientific reports* 9(1): 1–12.
- Itti, L.; and Koch, C. 2000. A saliency-based search mechanism for overt and covert shifts of visual attention. *Vision research* 40(10): 1489–1506.
- Itti, L.; and Koch, C. 2001. Computational modelling of visual attention. *Nature reviews neuroscience* 2(3): 194–203.
- Itti, L.; Koch, C.; and Niebur, E. 1998. A model of saliency-based visual attention for rapid scene analysis. *IEEE Transactions on pattern analysis and machine intelligence* 20(11): 1254–1259.
- Jarodzka, H.; Holmqvist, K.; and Nyström, M. 2010. A vector-based, multidimensional scanpath similarity measure. In *Proceedings of the 2010 symposium on eye-tracking research & applications*, 211–218.
- Judd, T.; Durand, F.; and Torralba, A. 2012. A Benchmark of Computational Models of Saliency to Predict Human Fixations. In *MIT Technical Report*.
- Kleiner, M.; Brainard, D.; and Pelli, D. 2007. Whats new in Psychtoolbox-3? Perception 36 ECVF Abstract Supplement. *PLOS ONE*.
- Knill, D. C.; and Pouget, A. 2004. The Bayesian brain: the role of uncertainty in neural coding and computation. *TRENDS in Neurosciences* 27(12): 712–719.
- Kotowicz, A.; Rutishauser, U.; and Koch, C. 2010. Time course of target recognition in visual search. *Frontiers in Human Neuroscience* 4: 31.
- Kummerer, M.; Wallis, T. S.; and Bethge, M. 2018. Saliency benchmarking made easy: Separating models, maps and metrics. In *Proceedings of the European Conference on Computer Vision (ECCV)*, 770–787.
- Kummerer, M.; Wallis, T. S.; Gatys, L. A.; and Bethge, M. 2017. Understanding low-and high-level contributions to



- fixation prediction. In *Proceedings of the IEEE International Conference on Computer Vision*, 4789–4798.
- Ma, W. J.; Navalpakkam, V.; Beck, J. M.; Van Den Berg, R.; and Pouget, A. 2011. Behavior and neural basis of near-optimal visual search. *Nature neuroscience* 14(6): 783.
- Meyniel, F.; Sigman, M.; and Mainen, Z. 2015. Confidence as bayesian probability: from neural origins to behavior. *Neuron* 88(1): 78–92.
- Najemnik, J.; and Geisler, W. S. 2005. Optimal eye movement strategies in visual search. *Nature* 434(7031): 387–391.
- Oliva, A.; and Torralba, A. 2006. Building the gist of a scene: The role of global image features in recognition. *Progress in brain research* 155: 23–36.
- O'Reilly, J. X.; Jbabdi, S.; and Behrens, T. E. 2012. How can a Bayesian approach inform neuroscience? *European Journal of Neuroscience* 35(7): 1169–1179.
- Rasouli, A.; and Tsotsos, J. K. 2014. Visual saliency improves autonomous visual search. In *2014 Canadian Conference on Computer and Robot Vision*, 111–118. IEEE.
- Riche, N.; Duvinage, M.; Mancas, M.; Gosselin, B.; and Dutoit, T. 2013. Saliency and human fixations: State-of-the-art and study of comparison metrics. In *Proceedings of the IEEE international conference on computer vision*, 1153–1160.
- Rohe, T.; and Noppeney, U. 2015. Cortical hierarchies perform Bayesian causal inference in multisensory perception. *PLoS Biology* 13(2).
- Rolfs, M. 2015. Attention in active vision: A perspective on perceptual continuity across saccades. *Perception* 44(8-9): 900–919.
- Russell, B. C.; Torralba, A.; Murphy, K. P.; and Freeman, W. T. 2008. LabelMe: a database and web-based tool for image annotation. *International journal of computer vision* 77(1-3): 157–173.
- Samad, M.; Chung, A. J.; and Shams, L. 2015. Perception of body ownership is driven by Bayesian sensory inference. *PloS one* 10(2).
- Simonyan, K.; and Zisserman, A. 2014. Very deep convolutional networks for large-scale image recognition. arXiv. Preprint.
- Tatler, B. W.; Wade, N. J.; Kwan, H.; Findlay, J. M.; and Velichkovsky, B. M. 2010. Yarbus, eye movements, and vision. *i-Perception* 1(1): 7–27.
- Tenenbaum, J.; Griffiths, T.; and Kemp, C. 2006. Theory-based bayesian models of inductive learning and reasoning. *Trends in Cognitive Sciences* 10(7): 309–318.
- Torralba, A.; Oliva, A.; Castelano, M. S.; and Henderson, J. M. 2006. Contextual guidance of eye movements and attention in real-world scenes: the role of global features in object search. *Psychological review* 113(4): 766.
- Torralba, A.; and Sinha, P. 2001. Statistical context priming for object detection. In *Proceedings Eighth IEEE International Conference on Computer Vision. ICCV 2001*, volume 1, 763–770. IEEE.
- Turgeon, M.; Lustig, C.; and Meck, W. H. 2016. Cognitive aging and time perception: roles of bayesian optimization and degeneracy. *Frontiers in aging neuroscience* 8: 102.
- Ullman, S. 2019. Using neuroscience to develop artificial intelligence. *Science* 363(6428): 692–693.
- Wiecki, T. V.; Poland, J.; and Frank, M. J. 2015. Model-based cognitive neuroscience approaches to computational psychiatry: clustering and classification. *Clinical Psychological Science* 3(3): 378–399.
- Yang, S. C.-H.; Wolpert, D. M.; and Lengyel, M. 2016. Theoretical perspectives on active sensing. *Current opinion in behavioral sciences* 11: 100–108.
- Yarbus, A. L. 1967. Eye movements during perception of complex objects. In *Eye movements and vision*, 171–211. Springer.
- Zhang, M.; Feng, J.; Ma, K. T.; Lim, J. H.; Zhao, Q.; and Kreiman, G. 2018. Finding any Waldo with zero-shot invariant and efficient visual search. *Nature communications* 9(1): 1–15.

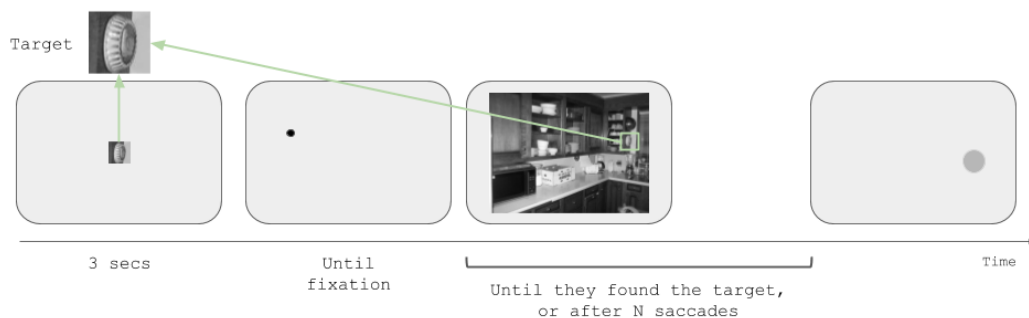
## Supplemental Information

### 1 Visual search in natural indoor images: Paradigm and human data acquisition and preprocessing

#### 1.1 Paradigm and procedure

We set up a visual search experiment in which participants have to search for an object in a crowded indoor scene. First, the target is presented in the center of the screen, subtending  $144 \times 144$  pixels of visual angle (Fig. S1). After 3 seconds, the target is replaced by a fixation dot at a pseudo-random position at least 300 pixels away from the actual target position in the image (Fig. S1). This is done to avoid starting the search close to the target. The initial position was the same for a given image and all participants. Moreover, the search image appears after the participant fixates the dot. Thus, all observers initiate the search in the same place for a given image. The image is presented at a  $768 \times 1024$  resolution (subtending  $28.3 \times 28.8$  degrees of visual angle) (Fig. S1).

The program automatically detects the end of each saccade during the target search. This period finishes when the participant fixates the target or after  $N$  saccades, allowing an extra 200ms for the participant to be able to process the information in that last fixation (Kotowicz, Rutishauser, and Koch, 2010). The maximum number saccades allowed ( $N$ ) varied between 2 (13.4% of the trials), 4 (14.9%), 8 (29.9%) or 12 (41.8%) for most of the participants (see Supplemental Information for details). These values were randomized for each participant, independently of the image.



Supplementary Figure S1: Paradigm schema

After each trial, the participants are forced to guess the position of the target, even if they had already found it. They are instructed to cover the target position with a Gaussian blur, first by clicking on the center and then by choosing its radius. This is done by showing a screen with only the frame of the image and a mouse pointer –a small black dot– to select the desired center of the blur (Fig. S1). When choosing a position with the mouse, a Gaussian blur centered at that position is shown, and the participants are required to indicate the uncertainty of their decision by increasing or decreasing the size of the blur using the keyboard. Position and uncertainty reports were not analyzed in the present study.

A training block of 5 trials was performed at the beginning of each session with the experimenter present in the room. After the training block, the experiment started and the experimenter moved

to a contiguous room. The images were shown in random order. Each participant observed the 134 images in three blocks. Before each block, a 9-point calibration was performed and the participants were encouraged to get a small break to allow them to rest between blocks. Moreover, each trial starts with the built-in drift correction procedure from the EyeLink Toolbox, in which the participant has to fixate in a central dot and hit the spacebar to continue. If the gaze is detected far from the dot, a beep signaled the necessity of a re-calibration. The experiment was programmed using PsychToolbox and EyeLink libraries in MATLAB (Brainard, 1997; Kleiner, Brainard, and Pelli, 2007).

## 1.2 Stimuli

We collected 134 indoor pictures from Wikimedia commons, indoor design blogs, and LabelMe database (Russell et al., 2008). The selection criterion was that scenes should have several objects and no human figures or text should be present. Moreover, the images are in black and white to make the task take more saccades, since color is a very strong bottom-up cue. Also, a pilot experiment with 5 participants was performed to select images that usually require several fixations to find the target. The original images were all larger or equal than  $1024 \times 768$  pixels, and all were cropped and/or scaled to  $1024 \times 768$  pixels. For each image, a single target was manually selected among the objects of  $72 \times 72$  pixels or less that were not repeated in the image –because we weren’t evaluating the accuracy of memory retrieval–. For all targets, we considered a surrounding region of  $72 \times 72$  pixels.

## 1.3 Data acquisition

Participants were seated in a dark room, 55cm away from a 19-inch Samsung SyncMaster 997MB monitor (refresh rate = 60Hz), with a resolution of  $1280 \times 960$ . A chin and forehead rest was used to stabilize the head. Eye movements were acquired with an Eye Link 1000 (SR Research, Ontario, Canada) monocular at 1000 Hz.

## 1.4 Data preprocessing

The saccade detection was performed online with the native EyeLink algorithm with the default parameters for cognitive tasks. Fixations were collapsed into a grid with cells of  $32 \times 32$  pixels, resulting in a grid size of  $32 \times 24$  cells. We explored the size of the grid in terms of model performance. Consecutive fixations within a cell were collapsed into one fixation to be fair with the model behavior. Also, fixations outside the image region were displaced to the closest cell. As we considered fixations, blinks periods were excluded.

The trial was considered correct (target found) if the participant fixated into the target region ( $72 \times 72$  pixels). Only correct trials were analyzed in terms of eye movements.

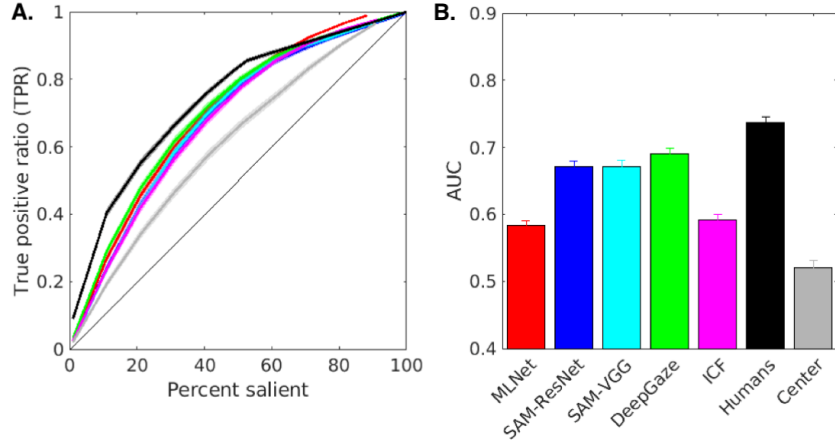
# 2 Exploring Saliency Maps

## 2.1 Comparing with other definitions of AUC

Different definitions of ROC-AUC found in <https://saliency.tuebingen.ai/> showed the same trend (Borji et al., 2013; Riche et al., 2013; Bylinskii et al., 2018; Kummerer, Wallis, and Bethge, 2018). All those ROC curves are built base on the idea of considering the saliency map as a binary classifier by applying a threshold. Here, we report three of them: AUC-Judd, AUC-Borji, and shuffled-AUC (or sAUC). These metrics differ mainly on the definition of the true positive rate and the false positive rate for the corresponding ROC curves. AUC-Judd considers human fixations as ground truth and all non-fixated pixels as negative cases. This way, the true positive rate is the proportion of pixels with saliency values above a certain threshold that were fixated. The false positive (fp) rate is the proportion of pixels with saliency values above a certain threshold that were not fixated. AUC-Borji keeps the same definition of the true positive rate, but uses a uniform random sample of image pixels as negatives and defines the saliency map values above a certain threshold at these pixels as false positives. Thus, the false positive rate is the proportion of those cases that were not fixated. Finally, sAUC is similar to AUC-Borji, instead of sampling pixels from the same image to define the fpr, it samples over fixation’s locations on other images.

Supplementary Table S1: Saliency maps: Different AUC metrics estimated for the saliency maps on the third fixation (Fig. 2)

Saliency Maps	AUC-Judd	AUC-Borji	sAUC
MLNet	0,7464	0,6797	0,6008
SAM-VGG	0,7321	0,6305	0,5666
SAM-ResNet	0,7339	0,6501	0,5820
DeepGaze 2	0,7637	0,6537	0,5883
ICF	0,7509	0,7078	0,5808
Humans	0,8076	0,7792	0,7727
Center	0,6866	0,6739	0,5208



Supplementary Figure S2: Saliency maps. **A)** ROC curves and **B)** AUC values for all fixations. Color mapping for models is consistent with Fig. 2.

## 2.2 Prediction of all fixation locations

## 3 Metrics on the Comparison of Performances between Humans and Models

We used three measures to compare the performance (i.e. the probability of detecting a target) of each model with the human participants. Each of them focused on a slightly different aspect.

### 3.1 Distance weighted by the number of saccades allowed

In order to directly compare the performance curve of each model with human participants, for each possible number of saccades allowed  $N \in \{2, 4, 8, 12\}$ , we calculate the difference between the mean proportion of targets found by participants and by the model  $m$  ( $P_{subj}(N)$  and  $P_m(N)$  respectively). For each number of saccades allowed, the difference is weighted by the standard deviation across participants  $\sigma$ . Then, the weighted distance  $WD(m)$  is the mean value each of those values:

$$WD(m) = \sum_{N \in \{2, 4, 8, 12\}} \frac{|P_{subj}(N) - P_m(N)|}{4\sigma^2} \quad (1)$$

### 3.2 Jaccard Index

Jaccard Index is a metric that allows us to measure the proportion of targets found by humans that are explained by the models. We represent each participant and each model as a boolean  $S$ -dimensional vector with a one in the  $i$ -th position if they found the target in the  $i$ -th image, and zero otherwise.  $S$  is the number of images: in our experiment,  $S = 134$ .

Every participant has the same proportion of images with each maximum saccade possible  $N$  (13.4% of the trials with  $N = 2$ , 14.9% with  $N = 4$ , 29.9% with  $N = 8$  or 41.8% with 12). Nonetheless, the subset that gets each  $N$  is chosen uniformly at random for each subject. This way, for each image we have subjects that were interrupted after 2, 4, 8, and 12 saccades. As each participant has a different sample of maximum saccades allowed across images, we apply these same constraints to the model. That is, when we want to compare with participant  $p$ , we apply their constraints to our model  $m$ . Then, we decide for each image if it can find the target in fewer saccades than the allowed. Given a model  $m$ , we define  $sacc(m, i)$  as the number of saccades that the model needs to find the target in the  $i$ -th image. Then, for each participant we have  $max\_sacc(i, p)$  as the number of saccades allowed for each image  $i$  and participant  $p$ , with  $p = 1 \dots 57$  in our data. From these values, we construct the vector of targets found by the model using the saccade threshold distribution for each participant  $p$ , called  $TFM_p^{(m)}$  (Targets Found by Model).  $TFM_p^{(m)} \in \{0, 1\}^S$  is defined as:

$$TFM_p^{(m)}(i) = \begin{cases} 1 & \text{if } sacc(m, i) \leq max\_sacc(i, p) \\ 0 & \text{otherwise} \end{cases} \quad (2)$$

Each participant  $p$  is also represented as a  $S$ -dimensional vector  $TFP_p \in \{0, 1\}^S$  (Targets Found by Participant):

$$TFP_p(i) = \begin{cases} 1 & \text{if participant } p \text{ found the target in the } i\text{-th image} \\ 0 & \text{otherwise} \end{cases} \quad (3)$$

Then, we compute the Jaccard Index (Real and Vargas, 1996) between those vectors (4).

$$jaccard(p, m) = \frac{TFP_p \cap TFM_p^{(m)}}{TFP_p \cup TFM_p^{(m)}} \quad (4)$$

### 3.3 Mean Agreement

Another measure we considered to compare a model performance against humans was what we called the Mean Agreement Score (MAS), inspired by Mean Absolute Error. This measure calculates the mean proportion of trials where both the participant and the model had the same performance. This metric has the purpose of measuring the compromise between our model and the participants in their performance. We compute the difference between the boolean vectors like in Jaccard Index (3) and calculate the mean. Finally the Mean Agreement Score between model  $m$  and participant  $p$  is 1 minus that value:

$$(5)$$

## 4 Scanpaths Examples

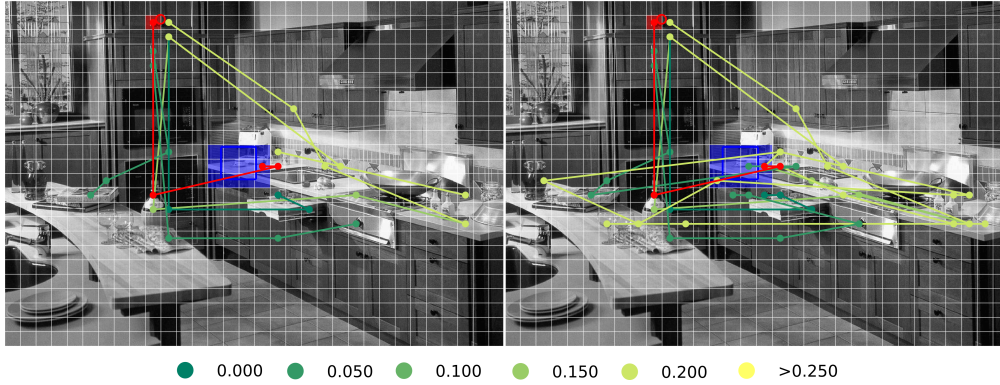
Some images showed an overall disagreement but, looking a little bit deeper, we can see that participants performed two different but consistent patterns. As the present implementation of the model is deterministic, it chose only one of those patterns (Figure S3). In Figure S3, we show some of the human scanpaths and the model (cIBS+DG2) scanpath for one image to illustrate that specific behavior. In this case, the cup is the search target and there are two surfaces where, a priori, is equally likely to find it. We selected six human scanpaths with different hmSD values to show how the initial decision determines the behavior and the overall hmSD for that scanpath (Fig. S3, left panel), but almost all participants end up exploring both regions (Fig. S3, right panel). Note that dark green traces are scanpaths very similar to the model, while yellow traces are scanpaths that differ from the model. Further development of the should focus on mimicking these individual differences in visual search.

## 5 Data and Code Availability

The model was fully developed in MATLAB. Saliency map calculations were performed using the public code provided by its respective authors (Cornia et al., 2016, 2018; Kummerer et al., 2017).



Image: 64 - bhSD: 0.15 - hmSD: 0.11



Supplementary Figure S3: Scanpath prediction comparison. The figure is meshed by a fixed grid of  $\delta = 32\text{px}$ . Each curve represents a scanpath, in red the cIBS+DG2 model's scanpath and six scanpaths of participants colored according to its own dissimilarity to the model scanpath. Left panel shows the first four fixations of each scanpath, and the right panel shows the whole scanpaths. The search target is represented with the blue square and the approximated first fixation with the red square. Above the image the hmSD and bhSD for this trial are reported. Image taken from *Wikipedia Commons*.

All code, data, and parameters needed to reproduce this paper's results and visualizations will be available in *GitHub*.

## References

- Borji, A.; Tavakoli, H. R.; Sihite, D. N.; and Itti, L. 2013. Analysis of scores, datasets, and models in visual saliency prediction. In *Proceedings of the IEEE international conference on computer vision*, 921–928.
- Brainard, D. H. 1997. The Psychophysics Toolbox. *Spatial Vision* 10: 433–436.
- Bylinskii, Z.; Judd, T.; Oliva, A.; Torralba, A.; and Durand, F. 2018. What do different evaluation metrics tell us about saliency models? *IEEE transactions on pattern analysis and machine intelligence* 41(3): 740–757.
- Cornia, M.; Baraldi, L.; Serra, G.; and Cucchiara, R. 2016. A deep multi-level network for saliency prediction. In *2016 23rd International Conference on Pattern Recognition (ICPR)*, 3488–3493. IEEE.
- Cornia, M.; Baraldi, L.; Serra, G.; and Cucchiara, R. 2018. Predicting human eye fixations via an lstm-based saliency attentive model. *IEEE Transactions on Image Processing* 27(10): 5142–5154.
- Kleiner, M.; Brainard, D.; and Pelli, D. 2007. What's new in Psychtoolbox-3? Perception 36 ECVF Abstract Supplement. *PLOS ONE*.
- Kotowicz, A.; Rutishauser, U.; and Koch, C. 2010. Time course of target recognition in visual search. *Frontiers in Human Neuroscience* 4: 31.
- Kummerer, M.; Wallis, T. S.; and Bethge, M. 2018. Saliency benchmarking made easy: Separating models, maps and metrics. In *Proceedings of the European Conference on Computer Vision (ECCV)*, 770–787.
- Kummerer, M.; Wallis, T. S.; Gatys, L. A.; and Bethge, M. 2017. Understanding low-and high-level contributions to fixation prediction. In *Proceedings of the IEEE International Conference on Computer Vision*, 4789–4798.
- Real, R.; and Vargas, J. M. 1996. The probabilistic basis of Jaccard's index of similarity. *Systematic biology* 45(3): 380–385.

- Riche, N.; Duvinage, M.; Mancas, M.; Gosselin, B.; and Dutoit, T. 2013. Saliency and human fixations: State-of-the-art and study of comparison metrics. In *Proceedings of the IEEE international conference on computer vision*, 1153–1160.
- Russell, B. C.; Torralba, A.; Murphy, K. P.; and Freeman, W. T. 2008. LabelMe: a database and web-based tool for image annotation. *International journal of computer vision* 77(1-3): 157–173.